JOURNAL OF COMPUTATIONAL PHYSICS 70, 439–462 (1987)

A Pseudospectral Method for Solution of the Three-Dimensional Incompressible Navier–Stokes Equations

HWAR C. KU, RICHARD S. HIRSH, AND THOMAS D. TAYLOR

The Johns Hopkins University Applied Physics Laboratory, Laurel, Maryland 20707

Received April 25, 1986; revised September 19, 1986

A new Chebyshev pseudospectral technique (based on the projection method that was previously applied by the authors to the solution of two-dimensional incompressible Navier–Stokes equations in primitive variables for nonperiodic boundary conditions) is extended to solve the three-dimensional Navier–Stokes equations. The crucial point of the method is the requirement that the continuity equation be satisfied everywhere in the domain, on the boundaries as well as in the interior. The key feature of the work presented in this paper is that the computer storage requirements of the full matrix inversion resulting from direct solution of the pressure Poisson equation in three dimensions is greatly reduced by considering an eigenfunction decomposition. The method was tested on a two-dimensional driven cavity flow and the results were compared with those of the most accurate finite-difference calculation. The three-dimensional driven cavity flow was then calculated at the same Reynolds numbers as the two-dimensional cases, i.e., Re = 100, 400, and 1000. In the calculated results, three-dimensional boundary effects were observed in all cases and became more apparent with increasing Reynolds number.

1. INTRODUCTION

A number of finite difference solutions of the three-dimensional incompressible Navier–Stokes equations have been presented. The formulations include vector stream function-vorticity by Mallinson and de Vahl Davis [1], velocity–vorticity by Dennis *et al.* [2], velocity-potential by Kim and Moin [3] and primitive variables by Goda [4], as well as an improved TEACH-2E code by Freitas *et al.* [5]. Although there are three different kinds of formulations, the one based on the primitive variable form appears to be the least complex for solving the three-dimensional Navier–Stokes equations. As a result, that is the approach used in the present paper.

The applicability of high accuracy pseudospectral (or spectral) methods to the solution of three-dimensional Navier–Stokes equations has been limited to problems that admit periodic pressure boundary conditions in one or more dimensions. The reason for this is that it permits one to reduce the complexity of solving for the pressure field. Fully periodic solutions were initially employed by Orszag

0021-9991/87 $3.00

and Patterson [6] as well as by Riley and Metcalfe [7]. Subsequently, flows without periodicity in one direction were considered by Orszag and Kells [8], Deville *et al.* [9], and Moin and Kim [10]. In this paper we extend the approach to flows without any periodic boundary conditions.

In a companion paper [11] the authors addressed techniques and boundary conditions that could be easily extended to three dimensions. The discussion in that paper provides a foundation for the material presented here and may serve to answer questions. From that investigation it was determined that the Chorin projection or time splitting method [12] with the continuity equation as the boundary condition for pressure produced accurate solutions for two-dimensional problems. Furthermore, the results suggested that use of the continuity boundary condition yielded a better solution than when the classical momentum-equation-derived Neumann boundary condition was employed for pressure. This reflects the fact that there is no natural pressure boundary condition other than a divergence-free field. The application of the continuity equation at the boundary permits one to satisfy the incompressibility constraint everywhere to machine accuracy. As a result of the success of the two-dimensional investigation, the authors have employed the same approach for a three-dimensional flow in this paper. We note that the influence matrix method of Kleiser and Schumann [13] yielded similar accuracy to the approach used in the paper on two-dimensional flows [11]; however, its extension to three-dimensional problems is more complicated and, therefore, was not considered here.

The splitting method used in this study, as in most primitive variable approaches, yields a three-dimensional Poisson equation for the pressure. This presents a problem, since applying a Chebyshev pseudospectral matrix approach to solve the equation results in a large full matrix to invert, in contrast to the sparse banded matrix generated by a finite difference approach. Thus, in order to make the pseudospectral approach competitive, improved techniques for solving the matrix problem are required. Methods are available that can overcome the difficulty associated with the matrix inversion. These can be cast into two main categories: (1) direct reduced storage solutions or (2) iteration schemes. The direct solutions incorporating matrix diagonalization have been used by Haidvogel and Zang [14] in the two-dimensional case, Haldenwang *et al.* [15] and Tan [16] in the three-dimensional case. The iteration schemes use preconditioning with a simple finite-difference predictor as displayed by Orszag [17] or a finite-element as shown by Deville and Mund [18] and then use the pseudospectral method as a corrector. Different iteration schemes such as Richardson, Chebyshev, conjugate gradient, and multigrid (Zang *et al.* [19]) are used to converge the iteration. For most of the research, however, the boundary conditions were restricted to those of Dirichlet, mixed, and less for Neumann type. A direct solution method for the equation using the pseudospectral matrix method [20] with the continuity equation as the pressure boundary condition is presented in this paper. The key advance is that the typical computer storage for a direct three-dimensional matrix inversion is greatly reduced from $O(N^6)$ to $O(N^3)$, where N denotes the number of grid points in one

direction. This facilitates running of the three-dimensional program on a microcomputer system.

The paper is divided into eight sections; the first being the Introduction. Section 2 includes the general formulation of the derivatives by the pseudospectral matrix technique and in Section 3, the physical problem with suitable boundary conditions is described. Section 4 addresses the detailed numerical procedure for solving the three-dimensional Navier–Stokes equations in the primitive variable form and in Section 5, a direct and fast real-space pressure Poisson solver is developed (in contrast to the spectral-tau method). Section 6 outlines the stability condition for the time step as well as computing time and the modified "cycle" concept is introduced to accelerate the solution to reach the steady state. Section 7 presents the results obtained using the new Poisson solver for a two-dimensional driven-cavity flow problem and compares them with the most accurate finite-difference method by Ghia *et al.* [21]. Section 8 gives the conclusions. In addition, calculations for the three-dimensional case at Reynolds numbers of 100, 400, and 1000 are presented.

2. Calculation of Derivatives by Using Matrix Multiplies

With the collocation points selected as $x_j = \cos[\pi(j-1)/N]$, a smooth function, $f(x)$, defined on $x \in [-1, 1]$ when expanded in Chebyshev polynomials has first and second derivatives, in discrete form [20], that are approximately by

$$f'(x_j) = \sum_{l=1}^{N+1} \hat{G}^{(1)}_{j,l} f_l \tag{1a}$$

$$f''(x_j) = \sum_{l=1}^{N+1} \hat{G}^{(2)}_{j,l} f_l, \tag{1b}$$

with $\hat{\mathbf{G}}^{(q)} = \mathbf{T}\mathbf{G}^{(q)}\hat{\mathbf{T}}$, $q = 1, 2$, and $\mathbf{G}^{(2)} = \mathbf{G}^{(1)}\mathbf{G}^{(1)}$, where $\mathbf{T}$, $\mathbf{G}^{(1)}$, $\hat{\mathbf{T}}$ is an $(N+1)\times(N+1)$ matrix with elements

$$T_{i,j} = \cos\frac{\pi(i-1)(j-1)}{N} \tag{2a}$$

$$G^{(1)}_{i,j} = \begin{cases} 0 & \text{if } i \geqslant j \text{ or } i+j \text{ is even} \\ (2(j-1)/C_i) & \text{otherwise } (C_1 = 2,\ C_i = 1 \text{ for } i \geqslant 2) \end{cases} \tag{2b}$$

and

$$\hat{T}_{i,j} = \frac{2}{N\bar{C}_i\bar{C}_j}\cos\frac{\pi(i-1)(j-1)}{N} \qquad (\bar{C}_1 = \bar{C}_{N+1} = 2,\ \bar{C}_i = 1 \text{ for } 1 < i < N+1). \tag{2c}$$

When the domain of interest is $[0, 1]$, the above expressions are modified as

shown in [22]. When a symmetry boundary condition applies at $x=0$, the derivatives of a function with $x\in[0, 1]$ are given by

$$f'(x_j)=\sum_{l=1}^{N/2+1}\hat{G}S_{j,l}^{(1)}f_l \tag{3a}$$

$$f''(x_j)=\sum_{l=1}^{N/2+1}\hat{G}S_{j,l}^{(2)}f_l, \tag{3b}$$

where

$$\hat{G}S_{j,l}^{(q)}=\begin{cases}\hat{G}_{j,l}^{(q)}+\hat{G}_{j,N+2-l}^{(q)}, & l<N/2+1\\ \hat{G}_{j,l}^{(q)}, & l=N/2+1\end{cases} \tag{4}$$

and $j=1,..., N/2+1$. When an antisymmetry condition at $x=0$ applies. Eq. (3) is replaced by

$$f'(x_j)=\sum_{l=1}^{N/2+1}\hat{G}A_{j,l}^{(1)}f_l \tag{5a}$$

$$f''(x_j)=\sum_{l=1}^{N/2+1}\hat{G}A_{j,l}^{(2)}f_l, \tag{5b}$$

where

$$\hat{G}A_{j,l}^{(q)}=\begin{cases}\hat{G}_{j,l}^{(q)}-\hat{G}_{j,N+2-l}^{(q)}, & l<N/2+1\\ \hat{G}_{j,l}^{(q)}, & l=N/2+1\end{cases} \tag{6}$$

and $j=1,..., N/2+1$.

Note that all the calculations are manipulated in physical space rather than in the spectral space. As indicated by Street *et al.* [23] the matrix-multiply approach (in Fortran) can be significantly faster than FFT's (in assembly language), when the number of collocation points in a direction does not exceed approximately 100.

3. Governing Differential Equations and Boundary Conditions

The three-dimensional cavity flow in a cubic box (Fig. 1) can be represented in terms of a primitive variable formulation. In Cartesian coordinates, the time-dependent Navier–Stokes equations in nondimensional form can be written as

$$\frac{\partial u}{\partial t}+u\frac{\partial u}{\partial x}+v\frac{\partial u}{\partial y}+w\frac{\partial u}{\partial z}=-\frac{\partial p}{\partial x}+\frac{1}{\mathrm{Re}}\nabla^2 u \tag{7a}$$

$$\frac{\partial v}{\partial t}+u\frac{\partial v}{\partial x}+v\frac{\partial v}{\partial y}+w\frac{\partial v}{\partial z}=-\frac{\partial p}{\partial y}+\frac{1}{\mathrm{Re}}\nabla^2 v \tag{7b}$$

$$\frac{\partial w}{\partial t}+u\frac{\partial w}{\partial x}+v\frac{\partial w}{\partial y}+w\frac{\partial w}{\partial z}=-\frac{\partial p}{\partial z}+\frac{1}{\mathrm{Re}}\nabla^2 w \tag{7c}$$

$$\frac{\partial u}{\partial x}+\frac{\partial v}{\partial y}+\frac{\partial w}{\partial z}=0, \tag{7d}$$

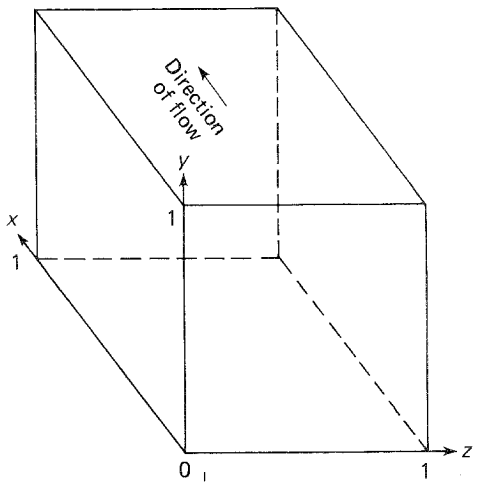

FIG. 1. Three-dimensional cavity flow configuration and coordinate system.

where

$$\nabla^2 = \frac{\partial^2}{\partial x^2} + \frac{\partial^2}{\partial y^2} + \frac{\partial^2}{\partial z^2}$$

and Re is the Reynolds number, $\rho Ul/\mu$, where ρ is the density, U is the velocity of the moving lid, l is the length of the cubic box, and μ is the viscosity.

Equations (7a)–(7d) are only solved for half of the cubic box due to the assumption of symmetry of the configuration about the plane $z = 0.5$. The initial and boundary conditions are given by, for $t > 0$,

$$u = v = w = 0 \qquad \text{at } x = 0 \quad \text{and} \quad x = 1 \tag{8a}$$

$$u = 1, \quad v = w = 0 \qquad \text{at } y = 1 \tag{8b}$$

$$u = v = w = 0 \qquad \text{at } y = 0 \tag{8c}$$

$$u = v = w = 0 \qquad \text{at } z = 1 \tag{8d}$$

$$\frac{\partial u}{\partial z} = \frac{\partial v}{\partial z} = \frac{\partial p}{\partial z} = 0, \quad w = 0, \qquad \text{at } z = 0.5 \tag{8e}$$

and for $t = 0$,

$$u = v = w = 0, \qquad 0 \leqslant x \leqslant 1, 0 \leqslant y \leqslant 1, 0 \leqslant z \leqslant 1. \tag{9}$$

The boundary conditions of Eqs. (8a) and (8b) will produce a jump in the solution at $x = 0$ and $x = 1$ at $y = 1$. In order to avoid this numerical complexity, the boundary conditions were adjusted over a few points so that at $x = 0$ and $x = 1$ the values were zero and at the next points on $y = 1$, $u = 0.3$, and 1.0, respectively. The

close spacing of the Chebyshev points near the boundary should make this approach a reasonable approximation to the original problem. A test was conducted to determine the sensitivity of the solution to this approximation. The value of 0.3 was increased to 0.5 and the impact was a third decimal place change in the interior solution at nearby grid points. As a result it was concluded that the approximation was adequate.

4. Formulation by the Pseudospectral Matrix Method

The method applied in this study is Chorin's [12] splitting technique. For this scheme, the equations of motion, in tensor form, are

$$\frac{\partial u_i}{\partial t}+\frac{\partial p}{\partial x_i}=F_i, \tag{10}$$

where $F_i=(1/\mathrm{Re})(\partial^2 u_i/\partial x_j^2)-u_j(\partial u_i/\partial x_j)$.

The first step in the method is to split the velocity into a sum of a predicted and corrected value. The predicted velocity field is determined by time integration of the momentum equations without the pressure terms in the form

$$\bar{u}_i^{n+1}-u_i^n=\Delta t F_i^n. \tag{11}$$

The second step is to develop the corrected velocity field that satisfies the continuity equation by using the relationships

$$u_i^{n+1}=\bar{u}_i^{n+1}-\Delta t\frac{\partial p}{\partial x_i} \tag{12a}$$

and

$$\frac{\partial u_i^{n+1}}{\partial x_i}=0. \tag{12b}$$

The discretization of Eqs. (12a) and (12b) by the aforementioned pseudospectral matrix method takes the form

$$u_{i,j,k}^{n+1}=\bar{u}_{i,j,k}^{n+1}-\Delta t\sum_{m=1}^{NX+1}\hat{G}X_{i,m}^{(1)}p_{m,j,k} \tag{13a}$$

$$v_{i,j,k}^{n+1}=\bar{v}_{i,j,k}^{n+1}-\Delta t\sum_{l=1}^{NY+1}\hat{G}Y_{j,l}^{(1)}p_{i,l,k} \tag{13b}$$

$$w_{i,j,k}^{n+1}=\bar{w}_{i,j,k}^{n+1}-\Delta t\sum_{n=1}^{NZ/2+1}\hat{G}S_{k,n}^{(1)}p_{i,j,n}. \tag{13c}$$

Note that only half of the grid points, $NZ/2+1$, are needed in the z direction due

to the geometric configuration. Hence z-dependent variables u, v, and p are expanded in a symmetric form, while w is expanded in an antisymmetric form. The resulting matrix forms have been indicated in Eqs. (3) and (5), respectively.

By requiring that the velocity components $u_{i,j,k}^{n+1}$, $v_{i,j,k}^{n+1}$, and $w_{i,j,k}^{n+1}$ satisfy the continuity equation throughout the whole domain, and with the incorporation of prescribed velocity boundary conditions (which were described in detail in [11, 24]), the substitution of Eqs. (13) into Eq. (12b) yields the following general form

$$\begin{aligned}\sum_{m=1}^{NX+1} BX_{i,m}p_{m,j,k} + \sum_{l=1}^{NY+1} BY_{j,l}p_{i,l,k} + \sum_{n=1}^{NZ/2+1} BZ_{k,n}p_{i,j,n} \\ = \frac{1}{\Delta t}\Bigg(\sum_{m=2}^{NX} \hat{G}X_{i,m}^{(1)} \bar{u}_{m,j,k}^{n+1} + \sum_{l=2}^{NY} \hat{G}Y_{j,l}^{(1)} \bar{v}_{i,l,k}^{n+1} + \sum_{n=2}^{NZ/2} \hat{G}A_{k,n}^{(1)} \bar{w}_{i,j,n}^{n+1} \\ + \hat{G}X_{i,1}^{(1)} u_{1,j,k}^{n+1} + \hat{G}X_{i,NX+1}^{(1)} u_{NX+1,j,k}^{n+1} + \hat{G}Y_{j,1}^{(1)} v_{i,1,k}^{n+1} \\ + \hat{G}Y_{j,NY+1}^{(1)} v_{i,NY+1,k}^{n+1} + \hat{G}A_{k,1}^{(1)} w_{i,j,1}^{n+1} + \hat{G}A_{k,NZ/2+1}^{(1)} w_{i,j,NZ/2+1}^{n+1} \Bigg)\end{aligned} \tag{14}$$

in the interior for $i=2,\ldots, NX$, $j=2,\ldots, NY$, and $k=2,\ldots, NZ/2+1$, where

$$BX_{i,m} = \sum_{p=2}^{NX} \hat{G}X_{i,p}^{(1)} \hat{G}X_{p,m}^{(1)} \tag{15a}$$

$$BY_{j,l} = \sum_{q=2}^{NY} \hat{G}Y_{j,q}^{(1)} \hat{G}Y_{q,l}^{(1)} \tag{15b}$$

and

$$BZ_{k,n} = \sum_{r=2}^{NZ/2} \hat{G}A_{k,r}^{(1)} \hat{G}S_{r,n}^{(1)}. \tag{15c}$$

At the boundaries, with prescribed velocity conditions where $i=1$ $(x=1)$ and $i=NX+1$ $(x=0)$, the supplemental pressure equation is related to the continuity equation, i.e., $\partial u/\partial x = -(\partial v/\partial y + \partial w/\partial z)$, so that

$$\begin{aligned}\sum_{m=1}^{NX+1} BX_{i,m}p_{m,j,k} = \frac{1}{\Delta t}\Bigg(\sum_{m=2}^{NX} \hat{G}X_{i,m}^{(1)} \bar{u}_{m,j,k}^{n+1} + \hat{G}X_{i,1}^{(1)} u_{1,j,k}^{n+1} + \hat{G}X_{i,NX+1}^{(1)} u_{NX+1,j,k}^{n+1} \\ + \sum_{l=1}^{NY+1} \hat{G}Y_{j,l}^{(1)} v_{i,l,k}^{n+1} + \sum_{n=1}^{NZ/2+1} \hat{G}A_{k,n}^{(1)} w_{i,j,n}^{n+1} \Bigg).\end{aligned} \tag{16a}$$

In the y direction, at $j=1$ $(y=1)$ and $j=NY+1$ $(y=0)$, i.e., $\partial v/\partial y = -(\partial u/\partial x + \partial w/\partial z)$, the supplemental pressure equation is

$$\begin{aligned}\sum_{l=1}^{NY+1} BY_{j,l}p_{i,l,k} = \frac{1}{\Delta t}\Bigg(\sum_{l=2}^{NY} \hat{G}Y_{j,l}^{(1)} \bar{v}_{i,l,k}^{n+1} + \hat{G}Y_{j,1}^{(1)} v_{i,1,k}^{n+1} + \hat{G}Y_{j,NY+1}^{(1)} v_{i,NY+1,k}^{n+1} \\ + \sum_{m=1}^{NX+1} \hat{G}X_{i,m}^{(1)} u_{m,j,k}^{n+1} + \sum_{n=1}^{NZ/2+1} \hat{G}A_{k,n}^{(1)} w_{i,j,n}^{n+1} \Bigg).\end{aligned} \tag{16b}$$

In an analogous manner, at $k=1$ ($z=1$), i.e., $\partial w/\partial z = -(\partial u/\partial x + \partial v/\partial y)$, we have

$$\sum_{n=1}^{NZ/2+1} BZ_{k,n} p_{i,j,n} = \frac{1}{\Delta t}\left(\sum_{n=2}^{NZ/2} \hat{G}A^{(1)}_{k,n} \bar{w}^{n+1}_{i,j,n} + \hat{G}A^{(1)}_{k,1} w^{n+1}_{i,j,1} + \hat{G}A^{(1)}_{k,NZ/2+1} w^{n+1}_{i,j,NZ/2+1} + \sum_{m=1}^{NX+1} \hat{G}X^{(1)}_{i,m} u^{n+1}_{m,j,k} + \sum_{l=1}^{NY+1} \hat{G}Y^{(1)}_{j,l} v^{n+1}_{i,l,k} \right). \tag{16c}$$

Equation (14), together with supplemental Eqs. (16) at the boundaries, constitutes the overall solution for the unknown pressure, with which continuity is satisfied to machine accuracy. What is more important, the pressure Poisson equation is a linear operator, and only an initial matrix inversion is required. The stored matrix inversion coefficients can then be used for all the following time steps to compute the pressure solution. Despite the advantage of the linear operator for the pressure equation, the remaining aspect is the challenge of how to solve the huge three-dimensional matrix without constraints on the size of the computer storage. This question is dealt with in Section 5.

5. A Direct and Fast Pressure Poisson Solver

The three-dimensional pressure Poisson equation can be solved either in real space of spectral space. Gottlieb and Orszag [25], Haidvogel and Zang [14], and Tan [16] employed a spectral space approach that is sometimes called the tau method. However, the real space pseudospectral solution approach seems to be more straightforward in dealing with boundary conditions. As a result, this is the approach adopted here. The method is similar to the tensor product method [26] used by Murdock [27] for two-dimensional flows in that eigenfunction expansions are used to reduce differential operators in the Poisson equation to algebraic relationships, but differs considerably in implementation. In this approach two spacial operators are reduced in the three-dimensional problem and the resulting one-dimensional second order equation is solved using a matrix method that has been previously described [22].

The method proceeds by first simplifying the right-hand sides of Eq. (14) and the supplemental pressure Eqs. (16) by defining a source term, $S_{i,j,k}$. Equation (14) then becomes

$$\sum_{m=1}^{NX+1} BX_{i,m} p_{m,j,k} + \sum_{l=1}^{NY+1} BY_{j,l} p_{i,l,k} + \sum_{n=1}^{NZ/2+1} BZ_{k,n} p_{i,j,n} = S_{i,j,k} \tag{17}$$

and the boundary conditions based on continuity take the form

$$\sum_{m=1}^{NX+1} BX_{i,m} p_{m,j,k} = S_{i,j,k}, \qquad i = 1, NX+1 \tag{18a}$$

$$\sum_{l=1}^{NY+1} BY_{j,l} p_{i,l,k} = S_{i,j,k}, \qquad j = 1, NY+1 \tag{18b}$$

and

$$\sum_{n=1}^{NZ/2+1} BZ_{k,n} p_{i,j,n} = S_{i,j,k}, \qquad k = 1. \tag{18c}$$

In order to develop an eigenfunction expansion with real eigenvalues for the operators in Eq. (17) it is necessary to first subtract out or remove boundary pressure terms. This can be accomplished in the x and y direction if one uses the continuity equation conditions given by Eqs. (18a) and (18b). From these equations, $p_{1,j,k}$, $p_{NX+1,j,k}$, $p_{i,1,k}$, and $p_{i,NY+1,k}$ can be expressed in terms of field variable in the interior, accordingly,

$$p_{1,j,k} = \Bigg[\sum_{m=2}^{NX} (BX_{NX+1,NX+1} BX_{1,m} - BX_{1,NX+1} BX_{NX+1,m}) p_{m,j,k} + BX_{1,NX+1} S_{NX+1,j,k} - BX_{NX+1,NX+1} S_{1,j,k} \Bigg] \Big/ (BX_{1,NX+1} BX_{NX+1,1} - BX_{NX+1,NX+1} BX_{1,1}) \tag{19a}$$

$$p_{NX+1,j,k} = \Bigg[\sum_{m=2}^{NX} (BX_{NX+1,1} BX_{1,m} - BX_{1,1} BX_{NX+1,m}) p_{m,j,k} + BX_{1,1} S_{NX+1,j,k} - BX_{NX+1,1} S_{1,j,k} \Bigg] \Big/ (BX_{NX+1,NX+1} BX_{1,1} - BX_{NX+1,1} BX_{1,NX+1}) \tag{19b}$$

and similarly,

$$p_{i,1,k} = \Bigg[\sum_{l=2}^{NY} (BY_{NY+1,NY+1} BY_{1,l} - BY_{1,NY+1} BY_{NY+1,l}) p_{i,l,k} + BY_{1,NY+1} S_{i,NY+1,k} - BY_{NY+1,NY+1} S_{i,1,k} \Bigg] \Big/ (BY_{1,NY+1} BY_{NY+1,1} - BY_{NY+1,NY+1} BY_{1,1}) \tag{20a}$$

$$p_{i,NY+1,k} = \Bigg[\sum_{l=2}^{NY} (BY_{NY+1,1} BY_{1,l} - BY_{1,1} BY_{NY+1,l}) p_{i,l,k} + BY_{1,1} S_{i,NY+1,k} - BY_{NY+1,1} S_{i,1,k} \Bigg] \Big/ (BY_{NY+1,NY+1} BY_{1,1} - BY_{NY+1,1} BY_{1,NY+1}). \tag{20b}$$

Substitution of Eqs. (19) and (20) into Eq. (17) gives

$$\sum_{m=2}^{NX} BX^*_{i,m}p_{m,j,k} + \sum_{l=2}^{NY} BY^*_{j,l}p_{i,l,k} + \sum_{n=1}^{NZ/2+1} BZ_{k,n}p_{i,j,n} = S^*_{i,j,k},$$
$$2 \leqslant k \leqslant NZ/2+1 \tag{21a}$$

and

$$\sum_{n=1}^{NZ/2+1} BZ_{k,n}p_{i,j,n} = S_{i,j,k}, \qquad k=1. \tag{21b}$$

Note the change of limits on the first two sums in Eq. (21a), as compared to Eq. (17). Here $S_{i,j,k} = S^*_{i,j,k}$ at $k=1$ and $BX^*_{i,m}$, $BY^*_{j,l}$, and $S^*_{i,j,k}$ are

$$\begin{aligned} BX^*_{i,m} = BX_{i,m} + [&BX_{i,NX+1}(BX_{NX+1,1}BX_{1,m} - BX_{1,1}BX_{NX+1,m}) \\ &- BX_{i,1}(BX_{NX+1,NX+1}BX_{1,m} - BX_{1,NX+1}BX_{NX+1,m})]/ \\ &(BX_{NX+1,NX+1}BX_{1,1} - BX_{NX+1,1}BX_{1,NX+1}) \end{aligned} \tag{22a}$$

$$\begin{aligned} BY^*_{j,l} = BY_{j,l} + [&BY_{j,NY+1}(BY_{NY+1,1}BY_{1,l} - BY_{1,1}BY_{NY+1,l}) \\ &- BY_{j,1}(BY_{NY+1,NY+1}BY_{1,l} - BY_{1,NY+1}BY_{NY+1,l})]/ \\ &(BY_{NY+1,NY+1}BY_{1,1} - BY_{NY+1,1}BY_{1,NY+1}) \end{aligned} \tag{22b}$$

and

$$\begin{aligned} S^*_{i,j,k} = S_{i,j,k} + [&BX_{i,1}(BX_{1,NX+1}S_{NX+1,j,k} - BX_{NX+1,NX+1}S_{1,j,k}) \\ &- BX_{i,NX+1}(BX_{1,1}S_{NX+1,j,k} - BX_{NX+1,1}S_{1,j,k})]/ \\ &(BX_{NX+1,NX+1}BX_{1,1} - BX_{NX+1,1}BX_{1,NX+1}) \\ &+ [BY_{j,1}(BY_{1,NY+1}S_{i,NY+1,k} - BY_{NY+1,NY+1}S_{i,1,k}) \\ &- BY_{j,NY+1}(BY_{1,1}S_{i,NY+1,k} - BY_{NY+1,1}S_{i,1,k})]/ \\ &(BY_{NY+1,NY+1}BY_{1,1} - BY_{NY+1,1}BY_{1,NY+1}). \end{aligned} \tag{22c}$$

We can now diagonalize the matrix BX^* of dimension $(NX-1)\times(NX-1)$ and the matrix BY^* of dimension $(NY-1)\times(NY-1)$ as

$$\mathbf{EX}^{-1}\mathbf{BX}^*\mathbf{EX} = \mathbf{\Lambda} \tag{23a}$$

and

$$\mathbf{EY}^{-1}\mathbf{BY}^*\mathbf{EY} = \chi, \tag{23b}$$

where $\mathbf{\Lambda}$ is a diagonal matrix of dimension $NX-1$ with diagonal elements α_i as the eigenvalues of the matrix $\mathbf{BX}^*$, and χ is a diagonal matrix of dimension $NY-1$ with diagonal elements β_j as the eigenvalues of the matrix $\mathbf{BY}^*$. The matrices $\mathbf{EX}$ and $\mathbf{EY}$ are the corresponding eigenvectors associated with each eigenvalue. The IMSL eigensystem routine EIGRF has been used for this in these computations.

If the solutions of pressure is expanded in a series of the eigenfunctions such that

$$\mathbf{P} = \mathbf{EX}\ \hat{\mathbf{P}}\ \mathbf{EY}^{\mathrm{T}} \tag{24a}$$

and the source term such that

$$\mathbf{S}^* = \mathbf{EX}\ \hat{\mathbf{S}}^*\ \mathbf{EY}^{\mathrm{T}}, \tag{24b}$$

where the superscript T denotes the transpose of the matrix, then the complete solution of pressure is obtained by a linear superposition of the eigenfunctions and its associated eigenvalues. Equations (24) are substituted into Eqs. (21) and, in view of Eqs. (23), Eqs. (21) are reduced to

$$\sum_{n=1}^{NZ/2+1} BZ_{k,n}\hat{p}_{i,j,n} + (\alpha_i + \beta_j)\,\hat{p}_{i,j,k} = \hat{S}^*_{i,j,k}, \qquad 2 \leqslant k \leqslant NZ/2+1 \tag{25a}$$

and

$$\sum_{n=1}^{NZ/2+1} BZ_{k,n}\hat{p}_{i,j,n} = \hat{S}^*_{i,j,k}, \qquad k = 1, \tag{25b}$$

for each $i = 2,..., NX$, $j = 2,..., NY$.

Equation (25a) with the boundary condition of Eq. (25b) represents a one-dimensional matrix inversion to find $\hat{p}_{i,j,k}$. The resulting pressure is then calculated using Eq. (24a). Note that all the matrix operations are simple one-dimensional matrix operations, which require much less computer storage than the three-dimensional system. Also all of the operational matrices **EX**, **EY**, $\mathbf{EX}^{\mathrm{T}}$, and $\mathbf{EY}^{\mathrm{T}}$, the eigenfunctions, and the solution of Eq. (25a) can be pretabulated and stored in the computer so that only matrix multiplies are required to compute the pressure at all future time steps.

The key feature of the technique is in the decomposition of the original three-dimensional matrix. Instead of the typical LU decomposition, eigenfunctions and eigenvalues have been used to decompose the matrix. As a result, in the final equation to be solved it is necessary to deal with a matrix of dimensions $(NZ/2+1)^2$ rather than one of $(NX)^2 \times (NY)^2 \times (NZ/2+1)^2$. The consequence of these steps has been to reduce the minimum storage requirements for direct matrix inversion from $O[(NX)^2(NY)^2(NZ/2+1)^2]$ to $O[(NX)(NY)(NZ/2+1)]$; i.e., the minimum storage requirement is no longer limited by the reduced matrix inversion, $O(N^2)$, but the storage of the field variables themselves, $O(N^3)$. This is an important result that permits use of much smaller computers to perform direct solution of the Poisson equation. One should note, however, that the reduced storage does not imply a large reduction in CPU operation count, but it does imply less storage access time, which is time-consuming in performing a calculation on a computer.

6. Computer Time and Time-Step Limitations

When using Chebyshev expansions in each direction for the computation of time-dependent problems, one can encounter a restricted time step for explicit time integration schemes as indicated in Eq. (11). For a diffusion-dominated problem, the critical time step is $O(\mathrm{Re}/N^4)$, while the critical time step for a convection-dominated case is $O(1/N^2)$.

By examining the splitting scheme adopted here, we find that the time constraint depends only on the first step and is independent of the second step, where continuity is satisfied by the pressure field. To determine the condition under which Eq. (11) is stable, consider the discrete L_2 norm of $\bar{u}_i^{n+1}$,

$$\|\bar{\mathbf{u}}^{n+1}\| \leqslant \|I - \delta t H(\mathbf{u}^n)\| \, \|\mathbf{u}^n\|, \tag{26}$$

where the operator H contains $u_j(\partial/\partial x_j) - (1/\mathrm{Re})(\partial^2/\partial x_j^2)$, $j = 1, 2, 3$.

Equation (26) is satisfied if

$$\delta t \leqslant O\left(\frac{1}{\begin{pmatrix}\max_{i,j,k}(|u_{i,j,k}^n|\, NX^2 + |v_{i,j,k}^n|\, NY^2 \\ \quad + |w_{i,j,k}^n|\, NZ^2) + (1/\mathrm{Re})(NX^4 + NY^4 + NZ^4)\end{pmatrix}}\right). \tag{27}$$

Note that Eq. (27) clearly indicates that the time step is restricted not only by the diffusion term but also by the convection term when $\mathrm{Re} \geqslant 100$. For the case of two-dimensional cavity flow, the time steps at $\mathrm{Re} = 100$ and 400 with 25×25 modes are 5×10^{-4} and 7×10^{-4}, respectively. At $\mathrm{Re} = 1000$ with 31×31 modes, the time step is 5×10^{-4}. To be specific, the two-dimensional case with 25×25 modes ran in 4.2 sec/time step and the 31×31 modes ran in 7.6 sec/time step on a VAX 11/750. Generally, in order to reach the steady state, it takes 15,000 to 30,000 times steps with increasing Reynolds number. In the case of three-dimensional driven cavity flow, the two-dimensional solutions were provided as initial conditions, and the same time step was used. The $25 \times 25 \times 13$ mode case runs in 11.1 sec/step for $\mathrm{Re} = 100$ or 400, and the $31 \times 31 \times 16$ case in 20.0 sec/step for $\mathrm{Re} = 1000$ on a VAX 11/780 with an FPS-164 array processor. Under these conditions it takes only 7,500 to 25,000 time steps to obtain the steady state solution.

At interesting test of the computations was made using a VAX performance analyzer. It showed that approximately 40% of the total CPU cost at each time step was used to compute the updated pressure and corrected velocity field. In order to reduce this, a technique similar to the subcycling technique proposed by Gresho *et al.* [28] may be used. In this technique, during every few steps (called a cycle) an approximate velocity field is estimated by using the pressure gradient extrapolated from the previous cycle, i.e., the true "current pressure" and the continuity equation is neglected during the cycle. At the end of each cycle, this slightly compressible flow is corrected through the regular procedure to insure that the incompressibility constraint is satisfied and the pressure gradient is updated. This

technique would be especially effective for slowly varying flows or those that approach steady state. The number of time steps that can be included in each cycle would have to be determined by testing and typically far less could be used at the early transient state than at the end of steady state. Note, however, that for the technique used in this paper the maximum speed-up using this approach would be less than 40%.

7. Results and Discussion

This section discusses the results obtained for the two- and three-dimensional cavity flows. First, computation of the flow in a two-dimensional square cavity

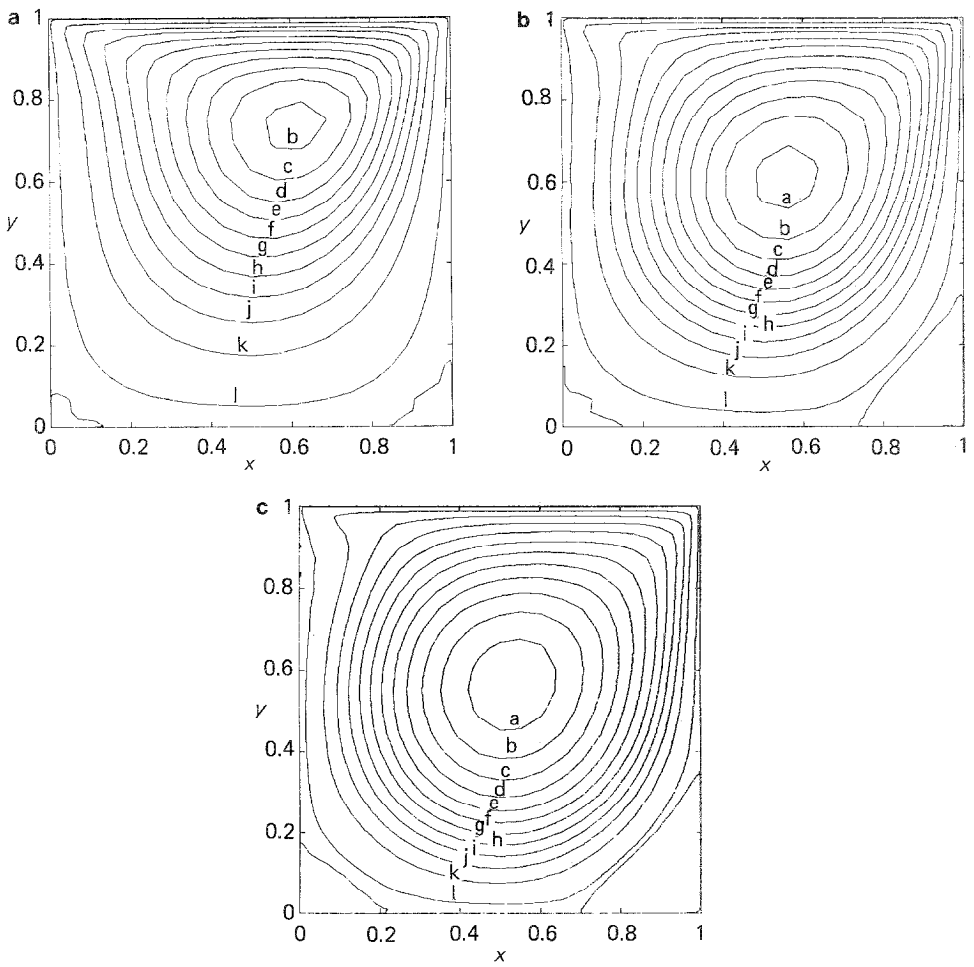

FIG. 2. Streamline pattern for Re = 100 with $\psi_{min} = -0.10367$; (a) contour letter $a = -0.11$, $b = -0.1$, $c = -0.09$, $d = -0.08$, $e = -0.07$, $f = -0.06$, $g = -0.05$, $h = -0.04$, $i = -0.03$, $j = -0.02$, $k = -0.01$, $l = -0.001$; (b) Re = 400 with $\psi_{min} = -0.11370$; (c) Re = 1000 with $\psi_{min} = -0.11619$.

using a primitive variable formulation is examined for Re = 100, 400, and 1000, and then results are compared with those of the most accurate finite-difference method in streamfunction voriticity formulation. Next, the results for a cubic cavity flow are presented for the same Reynolds numbers.

Since the technique for the three-dimensional case is essentially the same as that for the two-dimensional case, testing of the method on a two-dimensional square cavity flow for which other results exist makes it possible to ensure the validity of the present algorithm for a three-dimensional cavity flow. For the two-dimensional test 25×25 modes were chosen for Re = 100 and 400, and 31×31 modes for Re = 1000. Stream lines and velocity vectors for the driven cavity at these Reynolds numbers are shown in Figs. 2 and 3, respectively. The values of the minimum

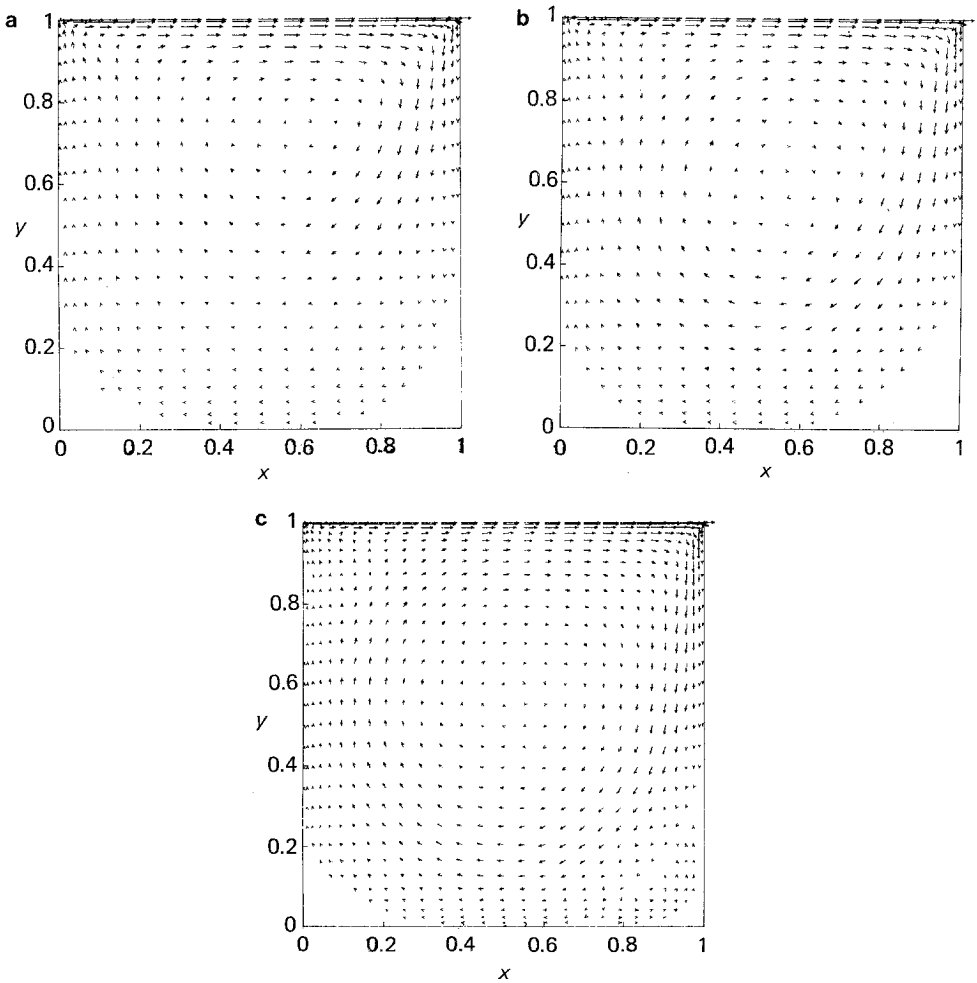

FIG. 3. Flow direction vectors for (a) Re = 100, (b) Re = 400, ((c) Re = 1000.

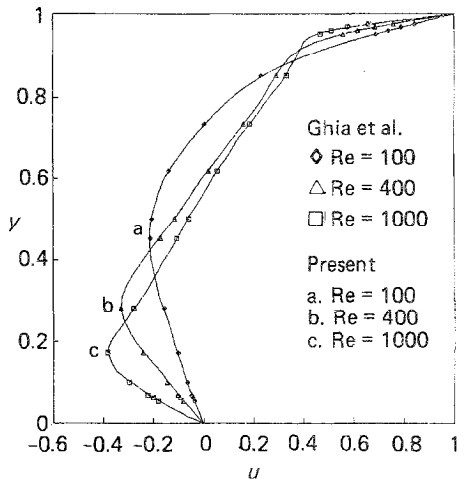

FIG. 4. Velocity profiles on vertical centerline of a square cavity.

streamfunction of the primary vortex center computed by the pseudospectral method are, with increasing Reynolds numbers, $\psi_{\min} = -0.10367$, -0.11370, and -0.11619. These are in good agreement with the fine grid results (129×129) reported by Ghia *et al.* [21] (i.e., $\psi_{\min} = -0.10342$, -0.11391, and -0.11793). These plots reproduce, in the lower corner region, small pockets of recirculating flow corresponding to positive dimensionless streamfunction values. Figures 4 and 5 show the plot of the profiles of both horizontal velocity along the vertical centerline and vertical velocity along the horizontal centerline for all the aforementioned Reynolds numbers. The present results agree well with those reported in [21] for all cases with agreement up to the third decimal place. This agreement indicates

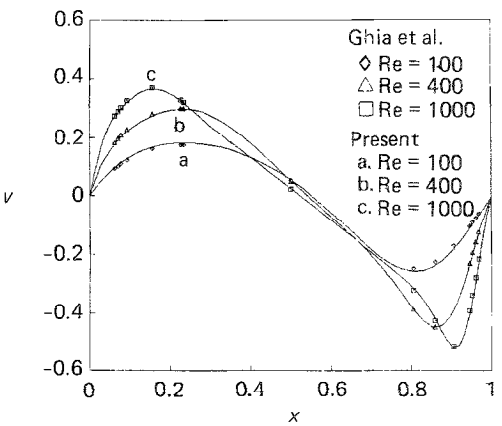

FIG. 5. Velocity profiles on horizontal centerline of a square cavity.

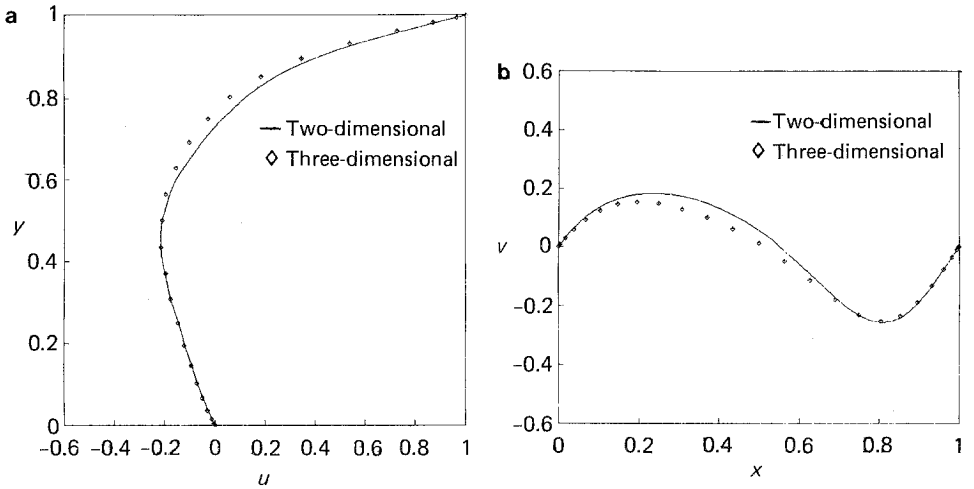

FIG. 6. Cubic cavity velocity profiles for Re = 100 on (a) vertical centerline, (b) horizontal centerline.

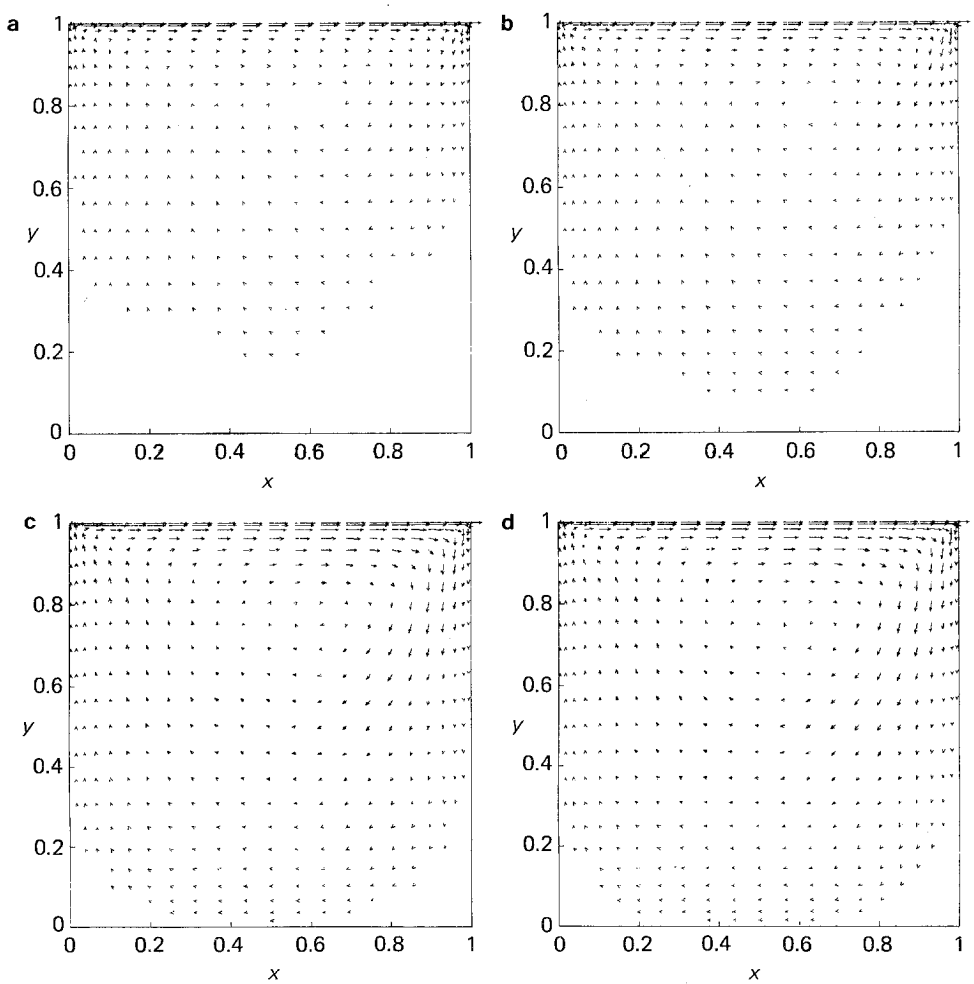

FIG. 7. Flow direction vectors for (a) Re = 100 in the $z = 0.982$ plane, (b) Re = 100 in the $z = 0.962$ plane, (c) Re = 100 in the $z = 0.75$ plane, and (d) Re = 100 in the $z = 0.5$ plane.

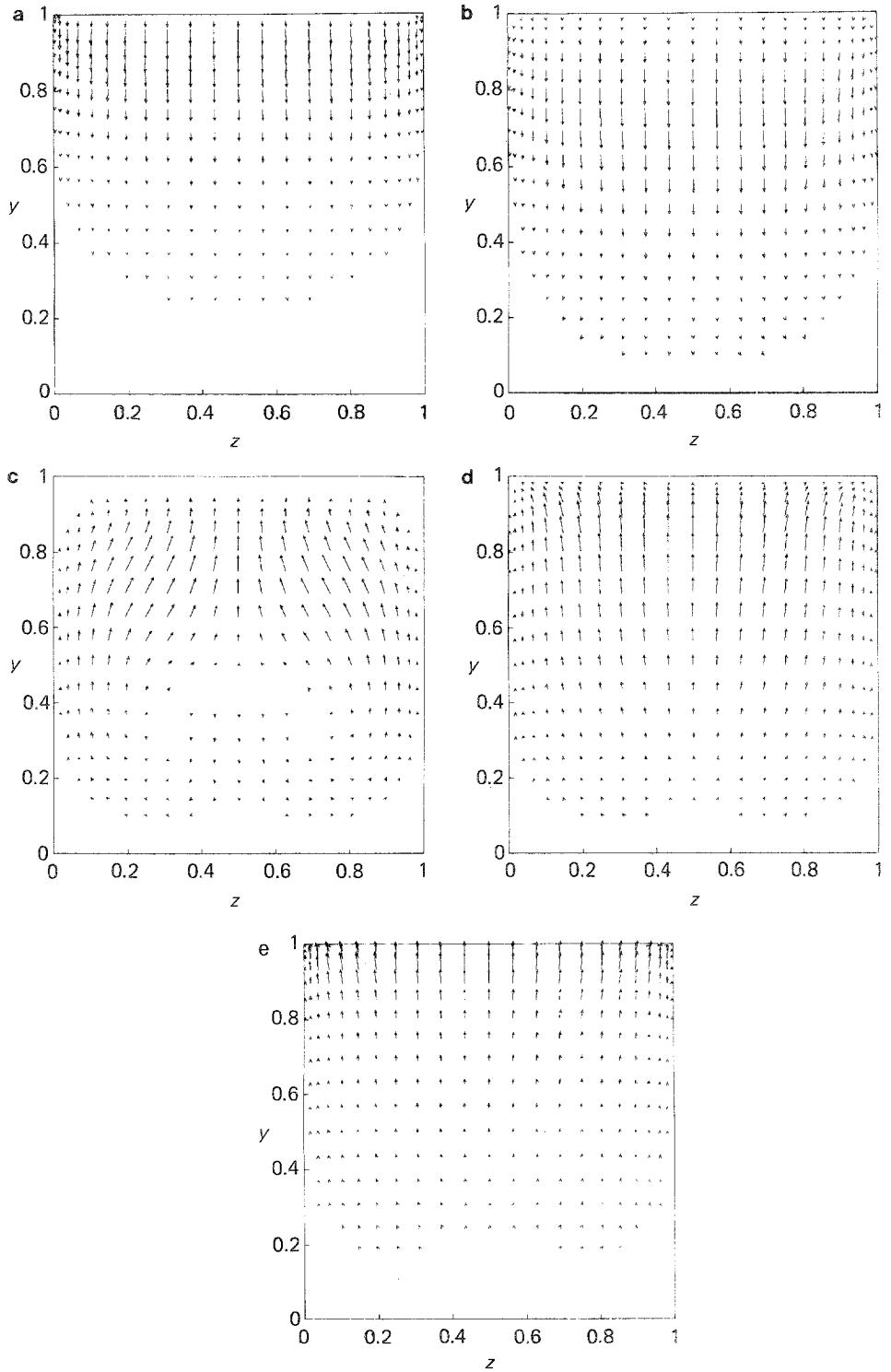

FIG. 8. Flow direction vectors for (a) $\mathrm{Re}=100$ in the $x=0.962$ plane, (b) $\mathrm{Re}=100$ in the $x=0.854$ plane, (c) $\mathrm{Re}=100$ in the $x=0.5$ plane, (d) $\mathrm{Re}=100$ in the $x=0.146$ plane, (e) $\mathrm{Re}=100$ in the $x=0.0381$ plane.

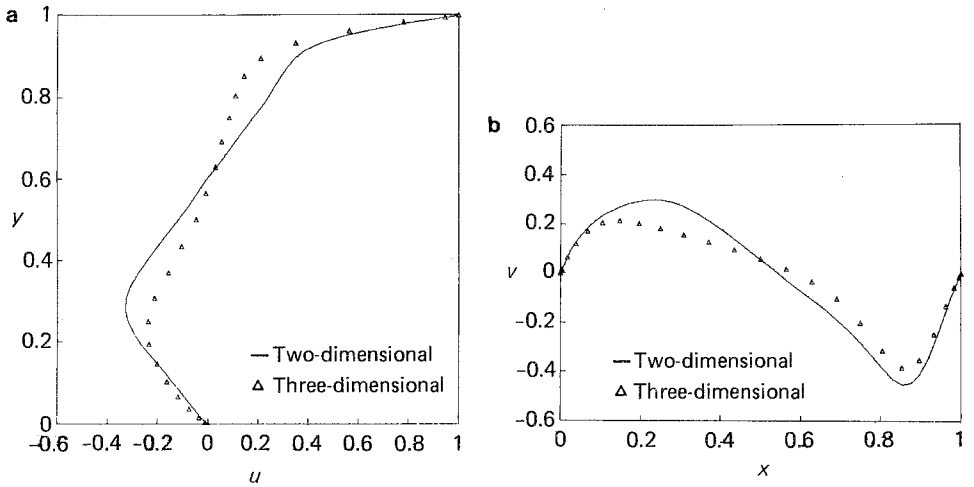

FIG. 9. Cubic cavity velocity profiles for Re = 400 on (a) vertical centerline, (b) horizontal centerline.

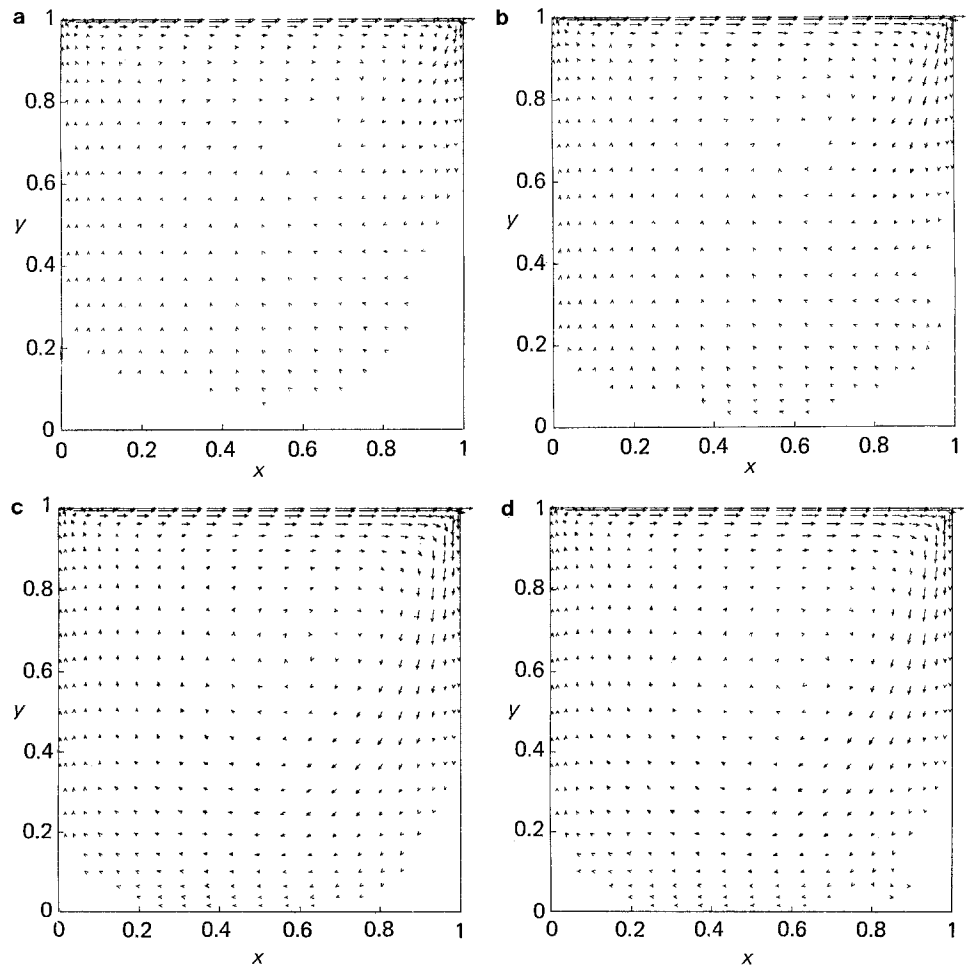

FIG. 10. Flow direction vectors for (a) Re = 400 in the $z = 0.982$ plane, (b) Re = 400 in the $z = 0.962$ plane, (c) Re = 400 in the $z = 0.75$ plane, and (d) Re = 400 in the $z = 0.3$ plane.

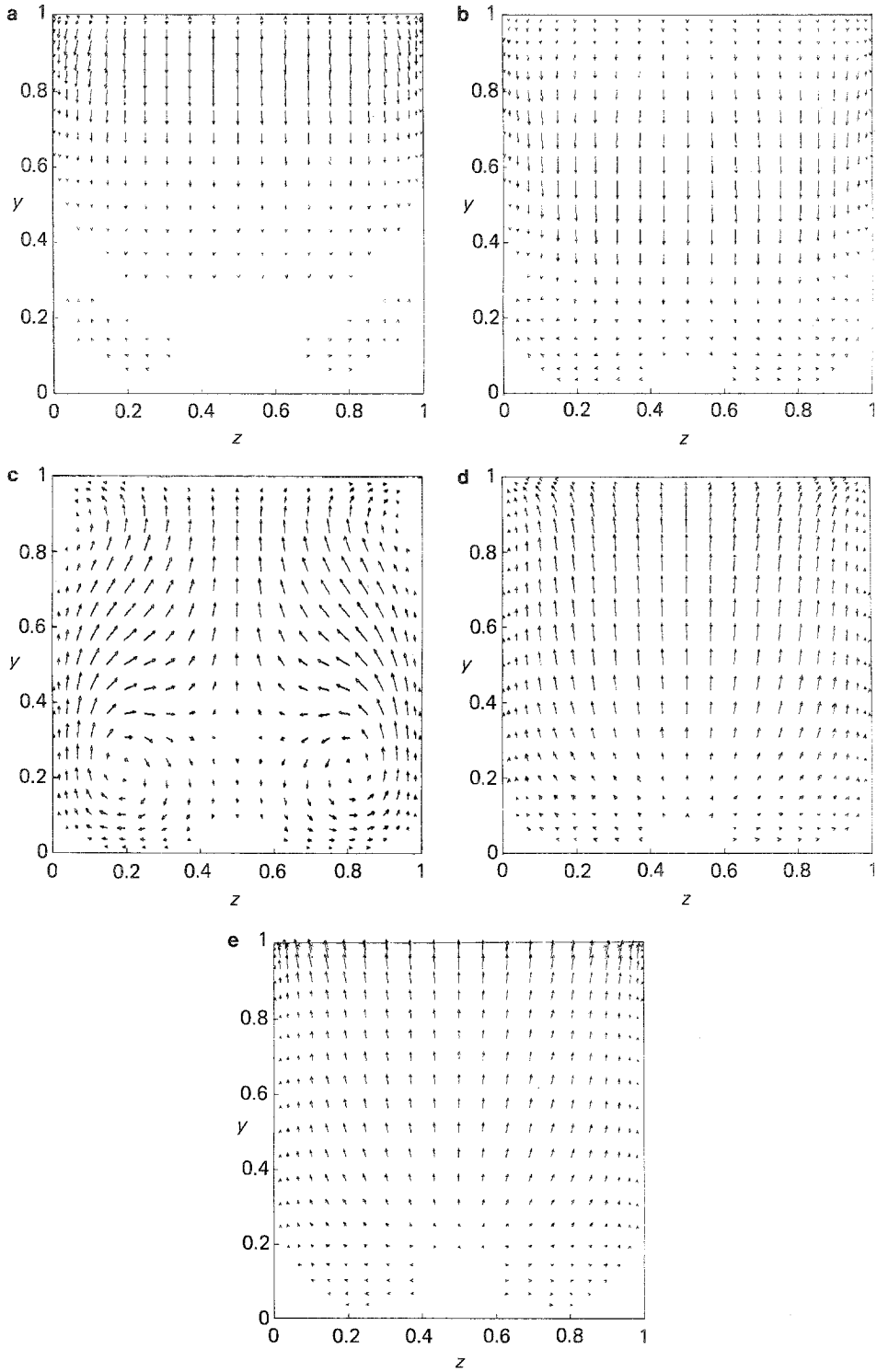

FIG. 11. Flow direction vectors for (a) $\mathrm{Re}=400$ in the $x=0.962$ plane, (b) $\mathrm{Re}=400$ in the $x=0.854$ plane, (c) $\mathrm{Re}=400$ in the $x=0.5$ plane, (d) $\mathrm{Re}=400$ in the $x=0.146$ plane, and (e) $\mathrm{Re}=400$ in the $x=0.0381$ plane.

that the resolution of thin boundary layers by the pseudospectral method is sufficiently high and gives confidence that the approach is correct and consistent. Once the test demonstrated the method for two dimension, the three-dimensional flow was tabulated.

Computational results for a three-dimensional cavity flow with Re = 100, 400, and 1000 are given in Figs. 6, 9, and 12. Displayed are the velocity profiles of the u component on the vertical centerline and the v component on the horizontal centerline of the plane $z = 0.5$. The two-dimensional results are shown for comparison. These plots clearly indicate that the three-dimensional boundary affects the flow even at low Reynolds numbers. In Fig. 9a and 9b for Re = 400, the flow motion is found to be reduced in strength compared to Re = 100. As expected, for a high Reynolds number Re = 1000), this boundary effect becomes more prominent, as shown in Figs. 12a and b. An attempt was made to compare the velocity results with those of Takami and Kuwahara [29] (Fig. 3) and Goda [4] (Figs. 8 and 9), but an exact comparison was not possible because of insufficient detail.

More details of the flow can be understood if we look at the flow structure in the different positions of the xy and yz planes. The xy plane velocity vector plots for Re = 100 and 400 at positions $z = 0.982$, 0.962, 0.75, and 0.5 are presented in Figs. 7a–d and Figs. 10a–d, respectively. Due to the boundary layer effect by the side wall, the results show that the deviation from the two-dimensional case is greatest near the side wall, as one would expect. Although flow patterns in the symmetry plane are similar to those of a two-dimensional flow, the strength is reduced. Similarly, the results for Re = 1000 at $z = 0.975$, 0.956, 0.75 and 0.5 in Figs. 13a–d show the same trend, except that the boundary layer effect is more pronounced.

The yz plane flow patterns for Re = 100 and 400 starting from the upstream to the downstream at $x = 0.962$, 0.854, 0.5, 0.146, and 0.0381 are plotted in Figs. 8a–e and Figs. 11a–e, respectively. Based on the plotted velocity vectors, one can easily

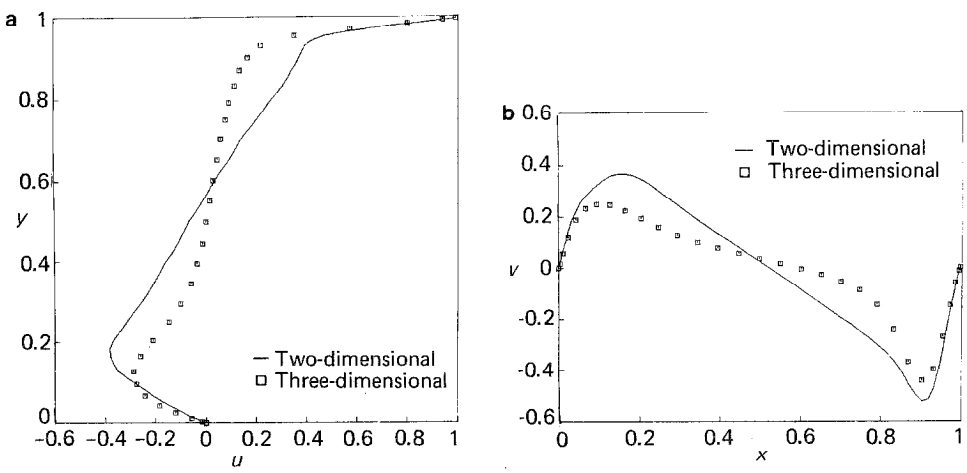

FIG. 12. Cubic cavity velocity profiles for Re = 1000 on (a) vertical centerline, (b) horizontal centerline.

distinguish whether the w component velocity flows inward or outward since without the w component velocity, the v component velocity should be vertical. Note that the flow patterns are not visible in some places due to very small values of both v and w. The vector plots are normalized by the largest vector in the plane displayed. As indicated in these figures for $0.5 \leqslant z \leqslant 1$, generally the w component velocity starts with an inward (negative) flow downstream and changes directions to an outward (positive) flow toward the upstream. For $\mathrm{Re} = 100$ in the downstream yz plane at $x = 0.854$, at the bottom a minor outward flow is observed, while for $\mathrm{Re} = 400$ at $x = 0.962$ and 0.854, a small recirculation flow is located at the bottom. In the yz plane at $x = 0.5$, two distinct secondary vortices are found that gradually shift toward the corners with increasing Reynolds numbers. For

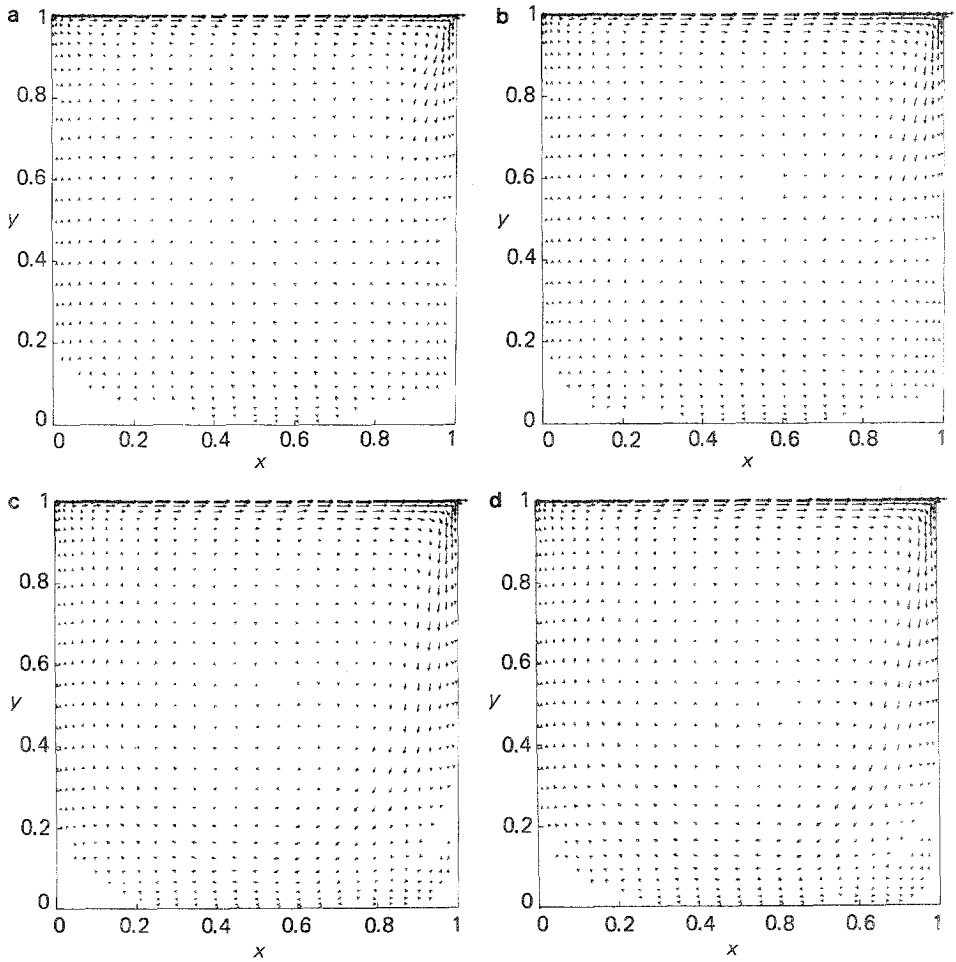

FIG. 13. Flow direction vectors for (a) $\mathrm{Re} = 1000$ in the $z = 0.975$ plane, (b) $\mathrm{Re} = 1000$ in the $z = 0.956$ plane, (c) $\mathrm{Re} = 1000$ in the $z = 0.75$ plane, and (d) $\mathrm{Re} = 1000$ in the $z = 0.5$ plane.

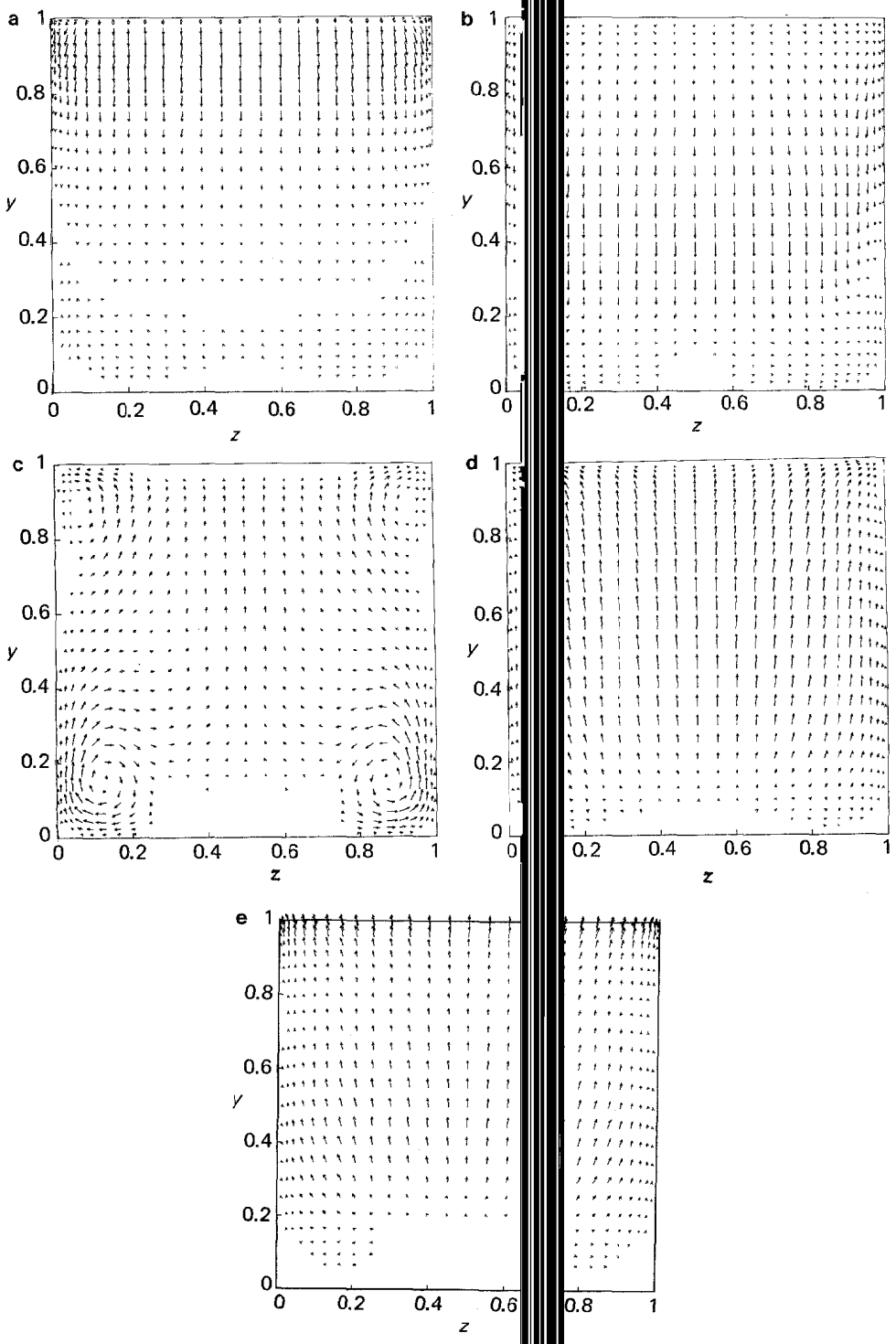

FIG. 14. Flow direction vectors for (a) $Re = 1000$ in t $= 0.975$ plane, (b) $Re = 1000$ in the $x = 0.871$ plane, (c) $Re = 1000$ in the $x = 0.5$ plane, (d) Re 00 in the $x = 0.129$ plane, and (e) $Re = 1000$ in the $x = 0.025$ plane.

$Re = 1000$, yz plane flow patterns are shown in Figs. 14a–e at $x = 0.975$, 0.871, 0.5, 0.129, and 0.025. The flow structure is similar except that two more small secondary vortices appear at the upper corner of the side walls, and the distortion of v component is more severe. The presence of Taylor–Görtler-like longitudinal vortices for $Re = 1000$ could not be established. For $Re > 1000$, their presence remains to be determined; this is a task for future study.

8. Conclusions

The three-dimensional Navier–Stokes equations using a primitive variable formulation have been solved by a Chebyshev pseudospectral matrix method for a three-dimensional driven-cavity flow by using a time-splitting technique. In the solution approach, the continuity equation is satisfied everywhere in the interior and on the boundaries, except at the corner singular points. This eliminates the need for momentum-equation-derived Neumann boundary conditions on the pressure.

The key feature of the work presented is that the resulting three-dimensional direct matrix inversion for the pressure Poisson equations is reduced to simple one-dimensional matrix operations by employing eigenfunction expansions. Since only one-dimensional matrices are involved, this formulation avoids the large storage normally associated with three-dimensional solutions of Poisson equations. The approach permitted storage of the overall inverted matrix coefficients that were applied during integration in the time domain using only the limited storage of a VAX 11/780.

Results for a two- and three-dimensional driven cavity flow have been compared for $Re = 100$, 400, and 1000. For all of the Reynolds numbers studied in this paper, Taylor–Görtler-like longitudinal vortices were not observed, and this topic remains an open question for $Re > 1000$.

Acknowledgments

The authors would like to thank Dr. J. L. Kerr and Mr. V. J. Sill for their assistance in running the computer program; and for the partial support of the Office of Naval Research under U.S. Navy Contract N00024-85-C-5301.

References

1. G. D. Mallinson and G. de Vahl Davis, *J. Fluid Mech.* **83**, 1 (1977).
2. S. C. R. Dennis, D. B. Ingham, and R. N. Cook, *J. Comput. Phys.* **33**, 398 (1979).
3. J. Kim and P. Moin, *J. Comput. Phys.* **59**, 308 (1985).
4. K. Goda, *J. Comput. Phys.* **30**, 76 (1979).
5. C. J. Freitas, R. L. Street, A. N. Findikakis, and J. R. Koseff, *Int. J. Numer. Methods Fluids* **5**, 561 (1985).

6. S. A. ORSZAG AND G. S. PATTERSON, *Phys. Rev. Lett.* **28**, 76 (1972).
7. J. J. RILEY AND R. W. METCALFE, AIAA paper 80-0274 (1980).
8. S. A. ORSZAG AND L. C. KELLS, *J. Fluid Mech.* **96**, 159 (1980).
9. M. DEVILLE, L. KLEISER AND F. MONTIGNY–RANNOU, *Int. J. Numer. Methods Fluids* **4**, 1149 (1984).
10. P. MOIN AND J. KIM, *J. Comput. Phys.* **35**, 381 (1980).
11. H. C. KU, T. D. TAYLOR AND R. S. HIRSH, *Comput. Fluids* (1987), in press.
12. A. J. CHORIN, *Math. Comput.* **22**, 745 (1968).
13. L. KLEISER AND U. SCHUMANN, in *Proceedings of the Third GAMM Conference on Numerical Methods in Fluid Mechanics*, edited by E. H. Hirschel (Vieweg and Sohn, Braunschweig, 1980), p. 165.
14. D. B. HAIDVOGEL AND T. ZANG, *J. Comput. Phys.* **30**, 167 (1979).
15. P. HALDENWANG, G. LABROSSE, S. ABBOUDI AND M. DEVILLE, *J. Comput. Phys.* **55**, 115 (1984).
16. C. S. TAN, *J. Comput. Phys.* **59**, 81 (1985).
17. S. A. ORSZAG, *J. Comput. Phys.* **37**, 70 (1980).
18. M. DEVILLE AND E. MUND, *J. Comput. Phys.* **60**, 517 (1985).
19. T. A. ZANG, Y. S. WANG AND M. Y. HUSSAINI, *J. Comput. Phys.* **48**, 485 (1982).
20. H. C. KU AND D. T. HATZIAVRAMIDIS, *J. Comput. Phys.* **56**, 495 (1984).
21. U. GHIA, K. GHIA AND C. A. SHIN, *J. Comput. Phys.* **48**, 387 (1982).
22. H. C. KU, T. D. TAYLOR AND D. T. HATZIAVRAMIDIS, in *Proceedings of the Sixth GAMM Conference on Numerical Methods in Fluid Mechanics*, edited by D. Rues and W. Kordulla (Vieweg and Sohn, Braunschweig, 1986), p. 201.
23. C. L. STREETT, T. A. ZANG, AND M. Y. HUSSAINI, *J. Comput. Phys.* **57**, 43 (1985).
24. T. D. TAYLOR AND H. C. KU, in *Proceedings of the International Symposium on Computational Fluid Dynamics, Tokyo* (Japan Society of Computational Fluid Dynamics, Tokyo, 1986), p. 262.
25. D. GOTTLIEB AND S. A. ORSZAG, *Numerical Analysis of Spectral Methods* (SIAM, Philadelphia, 1977).
26. R. E. LYNCH, J. R. RICE AND D. H. THOMAS, *Numer. Math.* **6**, 1985 (1964).
27. J. W. MURDOCK, *AIAA J.* **8**, 1167 (1977).
28. P. M. GRESHO, C. D. UPSON, S. T. CHAN AND R. L. LEE, in *Proceedings of the Fourth International Symposium on Finite Element Methods in Flow Problems*, edited by T. Kawai (North-Holland, Amsterdam, 1982), p. 786.
29. H. TAKAMI AND K. KUWAHARA, *J. Phys. Soc. Japan* **37**, 1695 (1974).